Applied Physics Letters ARTICLE pubs.aip.org/aip/apl

Performance degradation and *I–V* model of TiO_2-film-based resistive switching memory under proton irradiation

Cite as: Appl. Phys. Lett. **122**, 212102 (2023); doi: 10.1063/5.0147593
Submitted: 23 February 2023 · Accepted: 9 May 2023 ·
Published Online: 22 May 2023

View Online Export Citation CrossMark

Hongjia Song,[1,a)] Yingdong Liu,[1] Jiaqi Yan,[1] Xiangli Zhong,[1] Jinbin Wang,[1] and Hongxia Guo[2]

AFFILIATIONS

[1]School of Materials Science and Engineering, Xiangtan University, Xiangtan 411100, China
[2]State Key Laboratory of Intense Pulsed Radiation Simulation and Effect (Northwest Institute of Nuclear Technology), Xi'an 710024, China

[a)]Author to whom correspondence should be addressed: hjsong@xtu.edu.cn

ABSTRACT

The performance degradation of a TiO_2-film-based RRAM (resistive random access memory) is investigated in a proton irradiation experiment with an energy of 25 MeV. The results reveal that the fabricated Au/TiO_2 film/Ti devices exhibit typical *I–V* of bipolar resistive switching behavior under an irradiation of 1×10^{11} protons/cm^2. The low-resistance state (LRS) resistance remains nearly constant, but the high-resistance state (HRS) resistance decreases with an increasing proton fluence. The value of the HRS resistance decreases by approximately one order of magnitude when the value of proton fluence reaches 1×10^{11} protons/cm^2. Moreover, the SET voltage decreases with a decreasing proton fluence, while the RESET voltage remains almost constant. Material characterization via x-ray photoelectron spectroscopy demonstrates that the decrease in SET voltage and HRS resistance is mainly caused by radiation-induced oxygen vacancies and non-lattice oxygen. Based on the Voltage Threshold Adaptive Memristor model, a mathematical model of the *I–V* curve which demonstrates the variation in the RRAM resistance and voltage as a function of proton irradiation is constructed. The simulation results conformed to the experimental results under different proton fluences. Our results form a fundamental guide for the study of radiation performance degradation and radiation hardening of the RRAM with oxygen vacancy conducting filament.

As a key component in the high-performance next-generation nonvolatile memory that is essential for space equipment, the oxide-based RRAM (resistive random access memory) device has gained recent widespread attention.[1–5] Due to its simple metal/oxide/metal structure and memory mechanism based on an oxide-defect-based conductive filament, the RRAM device exhibits an ultra-high read/write speed, high density, low energy consumption, and high performance. Moreover, it is more resistant to defects caused by irradiation than conventional semiconductor devices.[6–9]

Resistive switching materials play a crucial role in the memory performance of these devices.[10] Among the many resistive switching materials, titanium oxide film has shown great promise in RRAM applications in recent years owing to its excellent memory characteristics, simple element composition, and good compatibility with CMOS technology.[11–14] Resistive switching based on TiO_2 films has been found to exhibit good radiation hardness.[15–18] Based on the proton irradiation, Vujisic *et al.* reported the effects of proton radiation, in the direction of a vertical platinum electrode, on the *I–V* characteristics and state retention of a titanium oxide memristor.[17] DeIonno *et al.*, through experiment and simulation, studied the effects of proton irradiation on titanium oxide memristor devices in a high resistance state (HRS), low resistance state (LRS), and growing state.[19–21] Liu *et al.* studied the performance degradation of the titanium oxide memristor subjected to proton irradiation with varying radiation energy, intensity, direction, angle, and duration.[22] The above studies reveal that: (i) Following proton irradiation, the HRS, LRS, SET (HRS to LRS), and RESET (shifting back to HRS from LRS) voltage, as well as the *I–V* characteristics, experience degradation. (ii) The impact of the different resistance states is miscellaneous. (iii) The effect varies with radiation energy, intensity, direction, angle, and duration of the proton. Therefore, further study is required on the degradation of the resistance and voltage of a device caused by proton irradiation for different resistance states. The *I–V* curve model serves as a reference for the analysis of the resistance mechanism and radiation damage

mechanism. However, the current reports of the *I–V* model under irradiation need to be developed in the *I–V* mode which can completely reflect the variety of the parameters of each resistive switching.

Herein, the radiation experiment involves irradiating a fabricated TiO_2-film-based RRAM under a proton source. The degradation of the voltage and resistance of this TiO_2-film-based RRAM following proton irradiation is analyzed. Additionally, the degenerate mechanism is further explored based on the results of the x-ray photoelectron spectrometer (XPS) analysis of the TiO_2 films prior to and after irradiation. Subsequently, a mathematical model of the *I–V* curve, with simultaneously varying voltage and resistance under proton irradiation, is established on account of the VTEAM (Voltage Threshold Adaptive Memristor) model.[23]

Figure 1(a) illustrates the composition of the TiO_2-film-based RRAM device. The TiO_2 film is the resistive switching layer, the top electrode of the device is composed of Au, and the base and bottom electrodes of the device are composed of titanium foil. The mask sputtering method was used to deposit Au on the top electrode of the upper surface of the TiO_2 switching layer. The diameter of the Au upper electrode is 200 μm, and its thickness is 30 nm. The area of the Ti foil is $25 \times 25 \times 0.5\ mm^3$. Its resistivity ranges from 0.1 to 0.5 $\mu\Omega$/m. The TiO_2 film with a thickness of 150 nm was coated on Ti substrates using a sol–gel method. Mixture A was formed by adding 10 ml of acetylacetone ($CH_3COCH_2COCH_3$,0.3 M) to 25 ml of 2-methoxy ethanol (MOE). This mixture was stirred for 30 min. Subsequently, tetra butyl titanate ($C_{16}H_{36}O_4Ti$,0.2 M) was added to mixture A to form solution B. Solution B was stirred for 5 h until its contents were completely dissolved. This yielded a clear TiO_2-film precursor solution. A titanium substrate was placed in a homogenizer, and the TiO_2 film precursor solution was dispensed slowly onto the substrate while the homogenizer was rotated for 10 s at 1000 rpm and 30 s at 3000 rpm. After coating the substrate with the precursor solution, the substrate was quickly placed on a platform at 250 °C to dry for 5 min and for removing moisture from the surface of the film. Afterwards, the pellicle was annealed in air at 480 °C for 15 min for releasing the residual organic matter in the film.

The performance degradation of the TiO_2-film-based RRAM subjected to proton radiation was examined. The protons had an energy of 25 MeV and a fluence rate of 10^7–10^8 cm^2/s. The final fluence was set at 1×10^{11} protons/cm^2. There were 100 devices exploited. Reference 23 shows that the 100 devices should be set to the HRS prior to irradiation because the HRS was more perceptive to irradiation. During irradiation, the devices exist in an unbiased state, and Ref. 18 shows that this is the principal working state.

An Agilent B1500A semiconductor parameter analyzer was used to test the performance of the resistive switching prior to and subsequent to device irradiation. In current–voltage (*I–V*) tests, the upper Au electrode was set to apply a voltage bias, and the titanium substrate was connected to the ground under ambient conditions. The valence electrons and compositions of the surface elements of the TiO_2 films were analyzed prior to and subsequent to irradiation using an x-ray photo-electron spectrometer (XPS, Thermo ESCALAB 250XI).

The *I–V* curves of the TiO_2-film-based RRAM were tested cycle-to-cycle under different proton fluences. The changing trend of the resistive switching parameters of the TiO_2-film-based RRAM is depicted in Figs. 1(b)–1(d). The representative *I–V* curves after irradiation are presented in these figures, with fluences of 1×10^{10}, 5×10^{10}, and 1×10^{11} protons/cm^2. The scanning voltage is $0 \rightarrow -2 \rightarrow 0 \rightarrow 2 \rightarrow 0$ V. In this process, the original device requires a forming process. Notably, the device maintains its HRS under different proton fluences

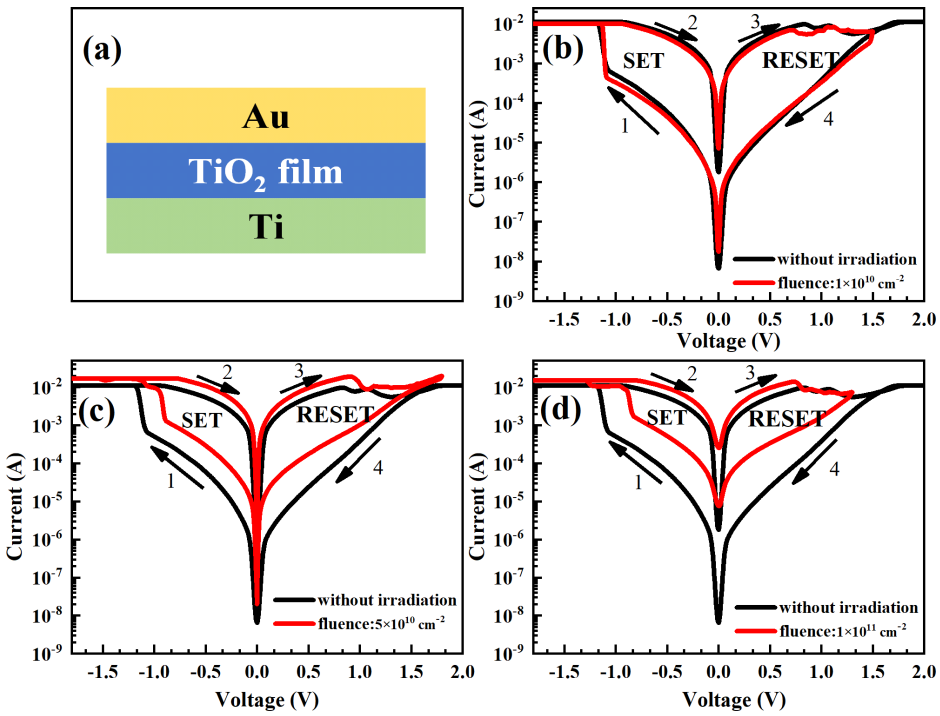

FIG. 1. *I–V* curves of TiO_2-film-based resistive switching memory before and after irradiation at a fluence of (a) schematic diagram of the memory, (b) 1×10^{10}, (c) 5×10^{10}, and (d) 1×10^{11} protons/cm^2.

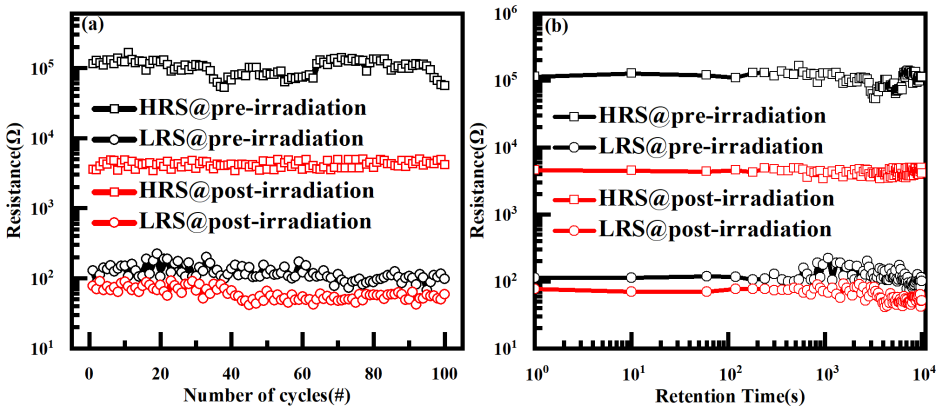

FIG. 2. (a) Endurance and (b) retention of the TiO_2-film-based resistive switching memory before and after irradiation.

and possesses the *I–V* curve of a bipolar resistive switching prior to and after radiation. The device has a SET voltage of approximately −1.1 V (shifting from HRS to LRS) and a RESET voltage of 0.9 V (shifting back to HRS). A clear distinction can be observed between devices in the HRS and LRS after radiation. The HRS/LRS resistance and RESET/SET voltage fluctuate as a function of radiation fluence. It is observed from Fig. 2 that the resistance devices possess stable endurance characteristics subsequent to irradiation, with the HRS/LRS resistivity having a value above 10^4 s.

The parameters of resistive switching between device-to-device were statistically analyzed to obtain the variation in resistance and the SET/RESET voltage as a function of irradiation fluence. The cumulative probability distributions of the SET and RESET voltages, as well as the resistances of the HRS and LRS, were obtained by examining the *I–V* curves of 100 resistive switching memories under varying proton fluences; these are depicted in Figs. 3(a) and 3(b). It is observed from Fig. 3(a) that the SET voltage decreases with an increasing proton fluence, but there is only a slight variation in the RESET voltage, and thus, it can be ignored. It is revealed from Fig. 3(b) that when the reading voltage is 0.1 V, the variation in the LRS resistance is insignificant. By contrast, the HRS resistance decreases with the addition of proton fluences. Moreover, when the proton fluence is 1×10^{11} protons/cm^2, the current in the HRS changes from 10^{-5} A to 10^{-4} A, a degradation of approximately one order of magnitude. Figures 4(a) and 4(b) depict the fitting lines of the SET voltage and HRS resistance as functions of proton fluence. A comparison between our resistance cell and other kinds of electrochemical metallization batteries and atomic switching devices reveals that the switching ratio of an electrochemical metallization battery subsequent to irradiation drops more severely than that of our machine.[24–27] However, the SET/RESET voltage does not fluctuate much.

In terms of mechanism analysis, we conducted an SRIM (Stopping and Range of Ions in Matter) simulation. The results demonstrate that all high-energy proton irradiations in this experiment pass through the TiO_2 thin film layer into the Ti bottom electrode/substrate, and the main energy loss observed is IEL (ionizing energy loss), accounting for more than 99.9% at 25 MeV. The energy of most of the secondary electrons is larger than the displacement threshold energy of the O atom in TiO_2, which implies that additional oxygen defects will be induced. Figure 5 illustrates the XPS spectra of the TiO_2 resistance layer prior to and subsequent to irradiation, which are used in analyzing the degradation of the resistive switching parameters due to proton fluence. Before irradiation, the peaks at 458.70 and 464.45 eV observed among the Ti 2p peaks are identified as Ti $2p_{3/2}$ and Ti $2p_{1/2}$, respectively, in the typical XPS spectra of Ti^{4+} in TiO_2. The Gaussian fitting peaks at 529.96 and 531.96 eV of O 1s are identified as the characteristic peaks of O^{2-} and non-lattice oxygen O^- in TiO_2, respectively. The intensities of the Gaussian fitting peaks of Ti $2p_{3/2}$, Ti $2p_{1/2}$, O^{2-}, and O^- decrease after irradiation, which indicates that irradiation can break the Ti–O bond in TiO_2. Some studies have demonstrated that this break will lead to an increase in oxygen vacancies.[28]

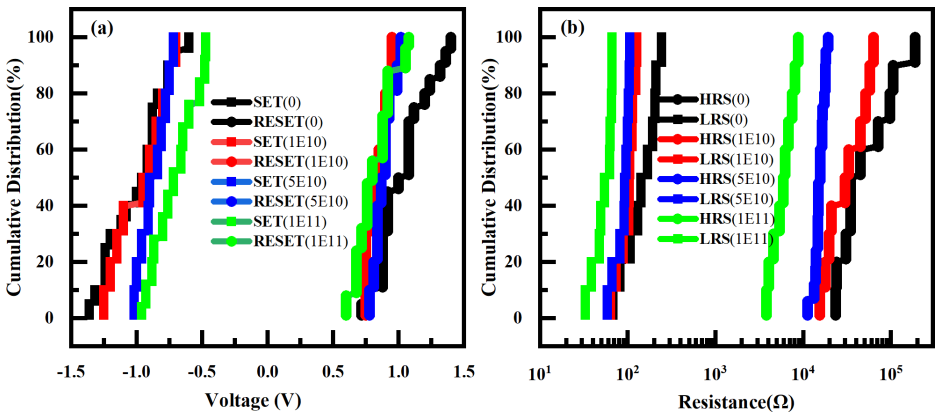

FIG. 3. Cumulative probability distribution of (a) SET/RESET voltage and (b) HRS/LRS resistance of the TiO_2-film-based resistive switching memory before and after irradiation. The number in parentheses represents the proton fluence.

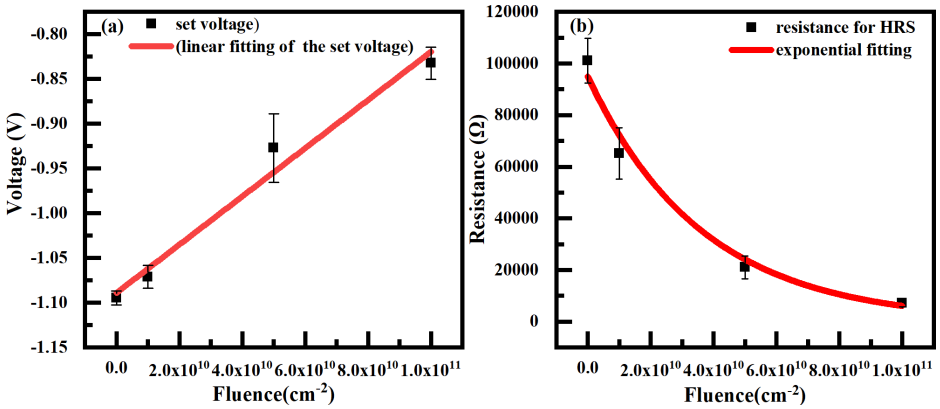

FIG. 4. (a) SET voltage and (b) HRS resistance of the TiO_2-film-based RRAM as functions of proton fluences.

The resistive switching mechanism in the TiO_2 film in our study is based on the oxygen vacancy conducting filament. Therefore, the resistance switching parameters of a device are affected by an increase in the oxygen vacancies.[29] Theoretically, the addition of oxygen vacancies in TiO_2 decreases the resistance of the HRS, thereby improving the conductivity.[30,31] It is observed from Figs. 3(b) and 4(b) that the results of the above analysis are consistent with the observed decreasing resistance and increasing proton fluence in the HRS. It is revealed from Fig. 3(b) that as the LRS is mainly affected by conductive filaments, oxygen vacancy conductive filaments have been formed in the LRS, and therefore, it has little influence on the LRS. Therefore, increasing oxygen vacancies does not significantly affect the LRS resistance. Figure 3(a) depicts that, for the SET voltage, due to the impact of radiation, oxygen vacancies increase in the TiO_2 functional layer. The addition of oxygen vacancies is conducive to the formation of conductive wires consisting of the oxygen vacancies themselves in the SET process. This makes it easier for conductive filaments to self-assemble and reduces the SET voltage.[31,32] Because of the formation of the conductive wires, a further increase in oxygen vacancies does not significantly impact the RESET voltage, and therefore, it remains almost constant.

By analyzing the increase in the oxygen vacancy of the resistive switching parameter as a function of proton fluence, a degradation model for the parameters of the resistive switching is constructed. As mentioned earlier, the increase in oxygen vacancies caused by irradiation enables the easy formation of conductive filaments and causes the SET voltage to decrease, thereby altering the operating voltage. The oxygen vacancies produced by irradiation in the oxide increase with an increasing radiation energy, such as the fluences of the proton.[33] Therefore, it can be inferred that the SET voltage decreases linearly with proton fluence:

$$V_{\mathrm{SET}} = \mathrm{a}x + b, \tag{1}$$

where V_{SET} represents the SET voltage, a represents the rate of change of the SET voltage augments with the addition of the proton fluences, x represents the proton irradiation fluence, and b represents the unirradiated SET voltage. Figure 4(a) depicts the fitting curve of the SET voltage.

In the RRAM device described in this study, the state variable w determines the resistance of the machine. The value of w is determined both by the level of oxygen defect migration and the oxygen defect density. w is the ratio of the depth of the doped zone of oxygen vacancy to the overall thickness of the oxide layer. An increase in w results in an increase in the oxygen vacancies caused by irradiation. Therefore, the I–V equation for the nonlinear migration of RRAM devices to oxygen vacancies can be presented as follows:[23]

$$I \propto \exp(w)V. \tag{2}$$

Consequently, the variation of the resistance of the HRS with the proton fluences x can be considered here

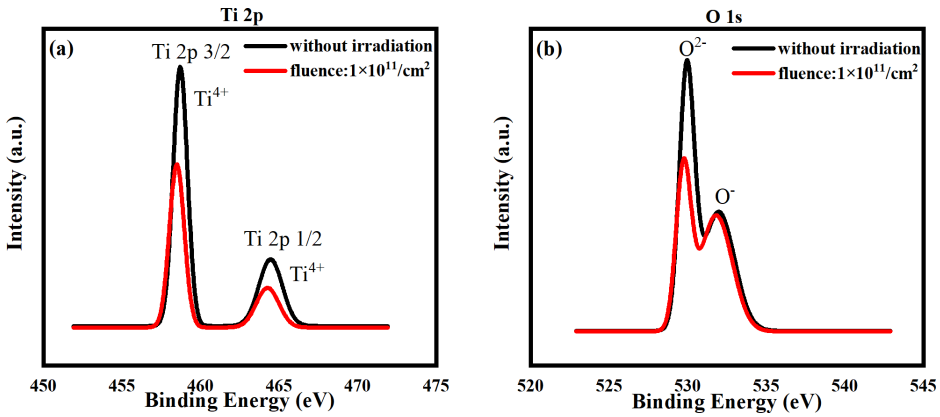

FIG. 5. X-ray photoelectron spectroscopy of the TiO_2 resistive switching layer: (a) XPS spectrum of Ti 2p and (b) XPS spectrum of O 1s.

$$R_{HRS} = c \times \exp(d \cdot x) + g, \tag{3}$$

where R_{HRS} represents the resistance of HRS, and c, d, and g are the fitting arguments. The fitting line is illustrated in Fig. 4(b). The fitting curve in Fig. 4(b) is almost consistent with the experimental data. In formula (3), g can be regarded as the threshold of the R_{HRS} value of our model. This implies that our model would prove to be incorrect if the R_{HRS} value is lower than the g value. In this study, the minimum g value is approximately 3300. It can be inferred that when the proton fluence reached 1.71×10^{13} protons/cm^2, the resistance value of the HRS of the device in our model decreased to approximately 3300 Ω, which is close to the minimum g value. Thus, the applicable range of fluence for our model is 0–1.71×10^{13} protons/cm^2. Furthermore, at a fluence of 1.71×10^{13} protons/cm^2, the R_{ON}/R_{OFF} ratio is approximately 20 in our model. In contrast to the results of previous experimental studies,[34] we found that when the fluence is approximately 2×10^{13} protons/cm^2, the R_{ON}/R_{OFF} ratio of the device drops to around 20, which is basically consistent with our prediction. Moreover, Ref. 35 reveals that the device fails when the fluence of the high-energy proton is 1×10^{14} protons/cm^2.

Based on the VTEAM (Voltage Threshold Adaptive Memristor) model, the proton irradiation degradation model of the RRAM devices is constructed using the relationship between Eqs. (1) and (3). In the general VTEAM model, the equation for the dynamics of the state variable w(t) can be expressed as

$$\frac{dw(t)}{dt} = \begin{cases} k_{off}\left(\frac{V(t)}{V_{RESET}} - 1\right)^{\alpha_{off}} f_{off}(w), & 0 < V_{RESET} \le V, \\ 0, & V_{SET} < V < V_{RESET}, \\ k_{on}\left(\frac{V(t)}{V_{SET}} - 1\right)^{\alpha_{off}} f_{on}(w), & V \le V_{SET} < 0, \end{cases} \tag{4}$$

where t is the time, and k_{off}, k_{on}, α_{off}, and α_{on} are the model fitting parameters, whose values are determined by the characteristics of the device itself. In general, k_{off} is positive, and k_{on} is negative. V_{SET} and V_{RESET} are the thresholds for the model's voltage, and V(t) is the voltage between the devices. $f_{off}(w)$ and $f_{on}(w)$ are the dependency relationships of the derivative of the state variable w(t) on w(t), namely, the window function of the model. At this point, the window function is the Joglekar window function, f(x) = 1 − (2x − 1)2p, where p is the degree of nonlinearity and is a positive integer.[36] In the VTEAM model, the current–voltage relationship is expressed as follows:

$$I(t) = \frac{e^{-\frac{\lambda}{w_{off} - w_{on}}(w - w_{on})}}{R_{LRS}} V(t), \tag{5}$$

where V(t) is the voltage passing through both ends of the device, and I(t) is the current that flows through the device. The parameters w_{on} and w_{off} represent the boundaries of the state variable w, namely the upper and lower boundaries, respectively; R_{LRS} is the resistance of the device at the boundary w_{on}, i.e., the low resistance; and λ is a fitting parameter that satisfies the following relation:

$$e^{\lambda} = R_{HRS}/R_{LRS}. \tag{6}$$

According to Eq. (6), the resistance in the VTEAM model can be expressed as

$$R(w) = \frac{R_{LRS}}{e^{-\frac{\lambda}{w_{off} - w_{on}}(w - w_{on})}}. \tag{7}$$

The proton irradiation degradation model in this paper is unlike the usual VTEAM model; V_{SET} and R_{HRS} are considered to vary with proton fluences based on the relationship between Eqs. (1) and (3).

Figure 6 displays the fitting results based on the I–V curve data from the experiment, with a fluence of 1×10^{11} protons/cm^2. In order to obtain the optimal fitting parameters of k_{off}, k_{on}, α_{off}, α_{on}, and p, Eq. (5) is used in the proton irradiation degradation model to fit the experimental I–V curve. The fitting parameters are connected to the material type, device structure, and manufacturing process. During fitting, the voltage scanning signal is regarded to be consistent with the actual voltage sweep signal for electrical properties, as illustrated in Fig. 6. The simulation results are in good agreement with the experimental results for the fitting parameters $k_{off} = 5 \times 10^{-9}$, $k_{on} = -80$, $\alpha_{off} = 0.01$, $\alpha_{on} = 3$, and $p = 2$. Therefore, assuming that the parameters of the I–V curve remain unchanged after irradiation, the experimental results reveal that the changes in V_{RESET} and R_{LRS} are negligible. A significant change is observed only in V_{SET} and R_{HRS}. The fitting curve in Fig. 6 corresponds very well with the test results.

A proton irradiation degradation model was established to simulate the I–V curve under different radiation fluences, and the results are illustrated in Figs. 7(a)–7(c). The illustration in the figure is the fitting diagram of the model and experimental results. R_{HRS} and V_{SET} decrease with an increasing proton fluence, which is consistent with the test results. The accuracy of our model has been calculated by comparing the actual experiment I–V with the simulated I–V based on the relative mean square error formula.[23] The relative RMS error of the device without irradiation and with fluences of 1×10^{10}, 5×10^{10}, and 1×10^{11} protons/cm^2 are determined to be 4.24%, 2.51%, 2.64%, and 3.39%, respectively. From the illustration in the insets of Fig. 7, it can be observed that the difference between the simulated I–V and actual experimental I–V stems from the RESET processes. This indicates that our model effectively simulates the degradation of the resistve switching parameters of a device. Simulation of an I–V curve is extremely

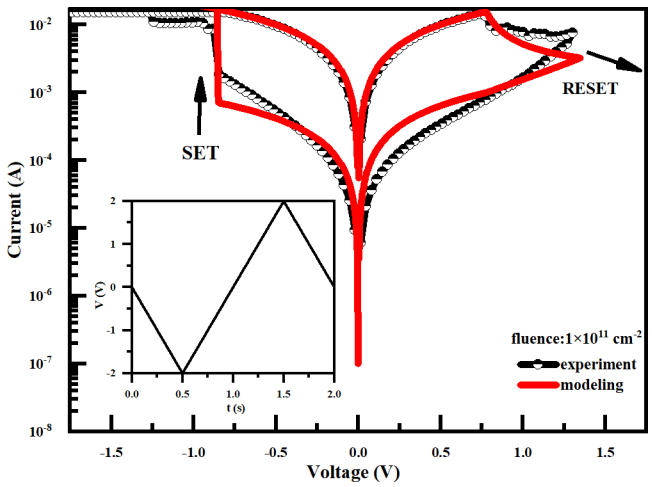

FIG. 6. Curve fitting of I–V characteristics for TiO_2-film-based RRAM devices at a fluence of 1×10^{11} protons/cm^2.

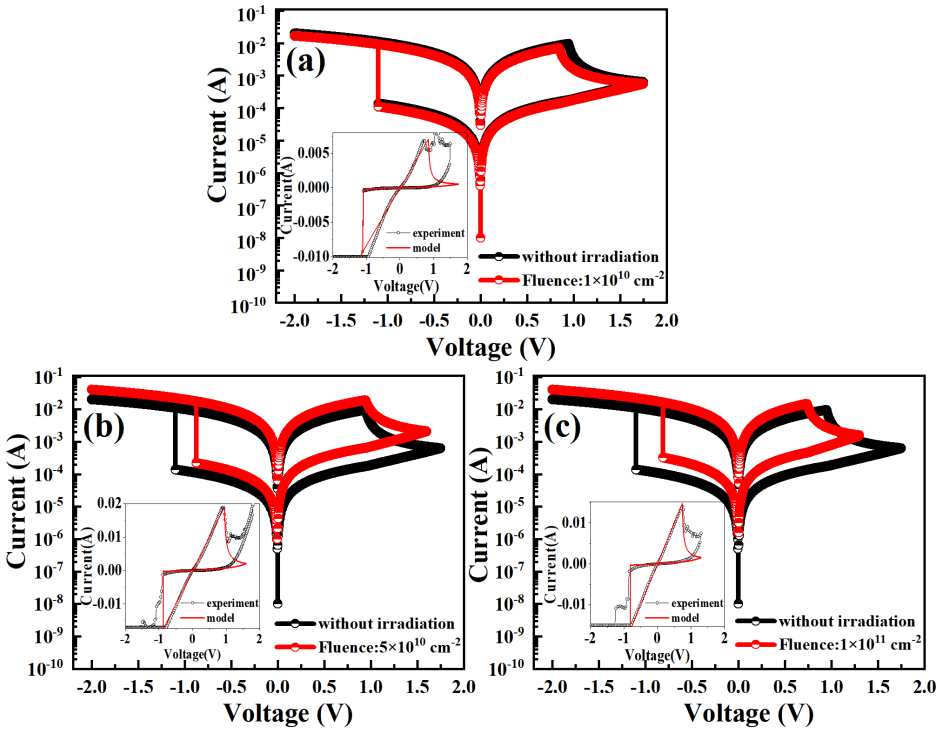

FIG. 7. Simulated *I–V* curves of TiO_2-film-based RRAM as functions of irradiation fluence: (a) 1×10^{10}, (b) 5×10^{10}, and (c) 1×10^{11} protons/cm^2. The insets show a comparison between the simulated *I–V* and actual experimental *I–V* with proton irradiation.

important in radiation hardening design. However, limited studies have been conducted on this topic. The model is also suitable for similar devices based on oxygen vacancy conductive filaments. First, relevant data were obtained at a low fluence to predict changes in R_{HRS}/R_{LRS} and V_{SET}/V_{RESET} at a high fluence. Second, degradation from proton irradiation can be expected according to the gain of oxygen vacancy. Nevertheless, the quantitative relationship between oxygen vacancies and radiation needs further study.

In summary, the degradation trend and degradation mechanism of proton irradiation were studied by using a TiO_2-film-based RRAM through a proton irradiation experiment of 25 MeV. The results showed that the TiO_2-film-based RRAM displayed typical *I–V* bipolar behavior at a fluence of 1×10^{11} protons/cm^2. The RESET voltage and the LRS resistance decreased slightly with an increasing proton fluence but remained constant overall. In contrast, the SET voltage and the HRS resistance decreased with an increasing proton fluence. The values of HRS resistance dropped by approximately one order of magnitude when the proton fluence reached 1×10^{11} protons/cm^2. XPS characterization of the resistive functional layer revealed that radiation-induced non-lattice oxygen and oxygen vacancies were the leading causes of the decrease in the SET voltage and HRS resistance. Using the VTEAM model as a guide, a mathematical model of the *I–V* curve that reflected the variation in resistance and voltage under proton irradiation was constructed, and the results proved to be almost consistent. Our research provides a reference guide for the study of radiation performance degradation and radiation hardening in the RRAM with oxygen vacancy conducting filament.

See the supplementary material for the additional Figs. s1–s4 and Table sI.

This work is supported by the Hunan Provincial Natural Science Foundation of China (No. 2021JJ30675), the National Natural Science Foundation of China (Nos. 12275230 and 12027813), the fund of innovation center of radiation application (No. KFZC2020020701), and the Special Fund of the State Key Laboratory of Intense Pulsed Radiation Simulation and Effect (No. SKLIPR1911).

AUTHOR DECLARATIONS

Conflict of Interest

The authors have no conflicts to disclose.

Author Contributions

Hongjia Song: Funding acquisition (equal); Supervision (equal); Writing – review & editing (equal). **Yingdong Liu:** Data curation (equal); Writing – original draft (equal). **Jiaqi Yan:** Data curation (equal). **Xiangli Zhong:** Supervision (equal). **Jinbin Wang:** Supervision (equal). **Hongxia Guo:** Supervision (equal).

DATA AVAILABILITY

The data that support the findings of this study are available from the corresponding author upon reasonable request.

REFERENCES

[1]C. Li, D. Belkin, Y. Li, P. Yan, M. Hu, N. Ge, H. Jiang, E. Montgomery, P. Lin, Z. Wang, W. Song, J. P. Strachan, M. Barnell, Q. Wu, R. S. Williams, J. J. Yang, and Q. Xia, Nat. Commun. **9**, 2385 (2018).
[2]S. Joshi, S. Wang, W. Savel'ev, R. Song, Y. Midya, M. Li, P. Rao, S. Yan, Y. Asapu, H. Zhuo, P. Jiang, C. Lin, J. H. Li, N. K. Yoon, J. Upadhyay, M. Zhang,

J. P. Hu, M. Strachan, Q. Barnell, H. Wu, R. S. Wu, Q. Williams, J. J. Xia, and Z. Yang, Nat. Electron. **1**, 137 (2018).
[3]H. S. P. Wong, H.-Y. Lee, S. Yu, Y.-S. Chen, Y. Wu, P.-S. Chen, B. Lee, F. T. Chen, and M.-J. Tsai, Proc. IEEE **100**, 1951 (2012).
[4]A. Sawa, Mater. Today **11**(6), 28 (2008).
[5]F. M. Simanjuntak, D. Panda, K. H. Wei, and T. Y. Tseng, Nanoscale Res. Lett. **11**, 368 (2016).
[6]C. M. M. Rosário, B. Thöner, A. Schönhals, S. Menzel, M. Wuttig, R. Waser, N. A. Sobolev, and D. J. Wouters, Appl. Phys. Lett. **112**, 213504 (2018).
[7]K. Agashe, N. Sarwade, S. Joshi, M. Thakurdesai, S. Surwase, P. Tirmali, and K. Asokan, Nucl. Instrum. Methods Phys. Res., Sect. B **403**, 38 (2017).
[8]A. Rodriguez-Fernandez, C. Cagli, J. Sune, and E. Miranda, IEEE Electron Device Lett. **39**, 656 (2018).
[9]N. Kanegami, Y. Nishi, and T. Kimoto, Appl. Phys. Lett. **116**, 013501 (2020).
[10]M. Lanza, H. S. P. Wong, E. Pop, D. Ielmini, D. Strukov, B. C. Regan, L. Larcher, M. A. Villena, J. J. Yang, L. Goux, A. Belmonte, Y. Yang, F. M. Puglisi, J. Kang, B. Magyari-Köpe, E. Yalon, A. Kenyon, M. Buckwell, A. Mehonic, A. Shluger, H. Li, T.-H. Hou, B. Hudec, D. Akinwande, R. Ge, S. Ambrogio, J. B. Roldan, E. Miranda, J. Suñe, K. L. Pey, X. Wu, N. Raghavan, E. Wu, W. D. Lu, G. Navarro, W. Zhang, H. Wu, R. Li, A. Holleitner, U. Wurstbauer, M. C. Lemme, M. Liu, S. Long, Q. Liu, H. Lv, A. Padovani, P. Pavan, I. Valov, X. Jing, T. Han, K. Zhu, S. Chen, F. Hui, and Y. Shi, Adv. Electron. Mater. **5**, 1800143 (2019).
[11]H. Shima, F. Takano, H. Muramatsu, H. Akinaga, I. H. Inoue, and H. Takagi, Appl. Phys. Lett. **92**, 043510 (2008).
[12]C. Rohde, B. J. Choi, D. S. Jeong, S. Choi, J.-S. Zhao, and C. S. Hwang, Appl. Phys. Lett. **86**, 262907 (2005).
[13]W. Wei, S. Fujita, and S. S. Wong, IEEE Electron Device Lett. **30**, 733 (2009).
[14]J. J. Yang, F. Miao, M. D. Pickett, D. A. Ohlberg, D. R. Stewart, C. N. Lau, and R. S. Williams, Nanotechnology **20**, 215201 (2009).
[15]M. Vujisic, K. Stankovic, N. Marjanovic, and P. Osmokrovic, IEEE Trans. Nucl. Sci. **57**, 1798 (2010).
[16]H. Abunahla, B. Mohammad, L. Mahmoud, M. Darweesh, M. Alhawari, M. A. Jaoude, and G. W. Hitt, IEEE Sens. J. **18**, 3198 (2018).
[17]Y. Abbas, R. B. Ambade, S. B. Ambade, T. H. Han, and C. Choi, Nanoscale **11**, 13815 (2019).
[18]A. Alessio, V. Bonino, T. Heisig, F. Picollo, D. Torsello, L. Mino, G. Martinez-Criado, R. Dittmann, and M. Truccato, Phys. Status Solidi RRL **15**, 2100409 (2021).
[19]E. DeIonno, M. D. Looper, J. V. Osborn, H. J. Barnaby, and W. M. Tong, in *IEEE Aerospace Conference Proceedings* (IEEE, Big Sky, MT, 2013).
[20]E. DeIonno, M. D. Looper, J. V. Osborn, and J. W. Palko, IEEE Trans. Nucl. Sci. **60**, 1379 (2013).
[21]E. DeIonno and A. L. White, in *IEEE Aerospace Conference Proceedings* (IEEE, Big Sky, MT, 2014).
[22]H.-J. Liu, X.-B. Tian, Q.-J. Li, Z.-L. Sun, and J.-T. Diao, Acta Phys. Sin. **64**, 078401 (2015).
[23]S. Kvatinsky, M. Ramadan, E. G. Friedman, and A. Kolodny, IEEE Trans. Circuits Syst. II **62**, 786 (2015).
[24]X. Guo, J. Liu, Q. Wang, and D. He, Microelectron. Eng. **231**, 111393 (2020).
[25]C. Su, L. Shan, D. Yang, Y. Zhao, Y. Fu, J. Liu, G. Zhang, Q. Wang, and D. He, Microelectron. Eng. **247**, 111600 (2021).
[26]N. Arun, K. V. Kumar, A. Mangababu, S. V. S. N. Rao, and A. P. Pathak, Radiat. Eff. Defects Solids **174**, 66 (2019).
[27]S. Petzold, S. U. Sharath, J. Lemke, E. Hildebrandt, C. Trautmann, and L. Alff, IEEE Trans. Nucl. Sci. **66**, 1715 (2019).
[28]H. Luo, Y. Liang, M. Tang, G. Li, Y. Xiong, Y. Sun, Y. Liu, S. Ouyang, Y. Xiao, S. Yan, W. Zhang, Q. Chen, and Z. Li, Microelectron. Reliab. **106**, 113592 (2020).
[29]D. Xue, H. Song, X. Zhong, J. Wang, N. Zhao, H. Guo, and P. Cong, J. Alloys Compd. **822**, 153552 (2020).
[30]D. R. Hughart, A. J. Lohn, P. R. Mickel, S. M. Dalton, P. E. Dodd, M. R. Shaneyfelt, A. I. Silva, E. Bielejec, G. Vizkelethy, M. T. Marshall, M. L. McLain, and M. J. Marinella, IEEE Trans. Nucl. Sci. **60**, 4512 (2013).
[31]R. Yang, Chin. Phys. B **29**, 097305 (2020).
[32]R. Ranjith, W. Prellier, J. Wei Cheah, J. Wang, and T. Wu, Appl. Phys. Lett. **92**, 232905 (2008).
[33]S. A. Yan, G. Li, W. Zhao, H. X. Guo, Y. Xiong, M. H. Tang, Z. Li, Y. G. Xiao, W. L. Zhang, Z. F. Lei, and Y. C. Zhou, Semicond. Sci. Technol. **30**, 085020 (2015).
[34]M. Ishfaq, M. R. Khan, M. F. Bhopal, F. Nasim, A. Ali, A. S. Bhatti, I. Ahmed, S. Bhardwaj, and C. Cepek, J. Appl. Phys. **115**, 147 (2014).
[35]D. Li, Y. Zhang, X. Tang, Y. He, and Y. Zhang, IEEE Access **8**, 104503 (2020).
[36]V. Mladenov and S. Kirilov, Electronics **6**, 77 (2017).